JGR Space Physics

RESEARCH ARTICLE
10.1029/2019JA027392

Reactions of the Middle Atmosphere Circulation and Stationary Planetary Waves on the Solar Activity Effects in the Thermosphere

A.V. Koval[1], N.M. Gavrilov[1], A.I. Pogoreltsev[1,2], and N.O. Shevchuk[1]

[1]Atmospheric Physics Department, Saint-Petersburg State University, Saint Petersburg, Russian Federation, [2]Meteorological Forecast Department, Russian State Hydrometeorological University, Saint Petersburg, Russian Federation

Key Points:
- Solar activity effects above 100 km may modify the mean temperature and zonal wind at heights below 100 km
- Impacts of solar activity in the thermosphere may significantly change amplitudes of stationary planetary waves in the middle atmosphere
- Amplitudes of planetary waves vary up to 50% in the thermosphere and 10–15% in the middle atmosphere.

Correspondence to:
A. V. Koval,
a.v.koval@spbu.ru

Citation:
Koval, A. V., Gavrilov, N. M., Pogoreltsev, A. I., & Shevchuk, N. O. (2019). Reactions of the middle atmosphere circulation and stationary planetary waves on the solar activity effects in the thermosphere. *Journal of Geophysical Research: Space Physics*, *124*, 10,645–10,658. https://doi.org/10.1029/2019JA027392

Received 29 SEP 2019
Accepted 20 NOV 2019
Accepted article online 15 DEC 2019
Published online 26 DEC 2019

Abstract Using numerical simulations of the general atmospheric circulation during boreal winter, statistically confident evidences are obtained for the first time, demonstrating that changes in the solar activity (SA) in the thermosphere at heights above 100 km can influence propagation and reflection conditions for stationary planetary waves (SPWs) and can modify the middle atmosphere circulation below 100 km. A numerical mechanistic model simulating atmospheric circulation and SPWs at heights 0–300 km is used. To achieve sufficient statistical confidence, 80 pairs of 15-day intervals were extracted from an ensemble of 16 pairs of model runs corresponding to low and high SA. Results averaged over these intervals show that impacts of SA above 100 km change the mean zonal wind and temperature up to 10% at altitudes below 100 km. The statistically confident changes in SPW amplitudes due to SA impacts above 100 km reach up to 50% in the thermosphere and 10–15% in the middle atmosphere depending on zonal wavenumber. Changes in wave amplitudes correspond to variations of the Eliassen-Palm flux and may alter dynamical and thermal SPW impacts on the mean wind and temperature. Thus, variable conditions of SPW propagation and reflection at thermospheric altitudes may influence the middle atmosphere circulation, thermal structure, and planetary waves.

Plain Language Summary Atmospheric large-scale disturbances, for instance planetary waves, play a valuable role in atmospheric general circulation, influencing its dynamical and thermal conditions. Solar activity might significantly change the mean temperature at heights above 100 km and alter conditions of wave propagation and reflection in the thermosphere. In the present study, we perform numerical simulations to obtain statistically confident results showing noticeable response of atmospheric circulation at altitudes below 100 km to impacts of solar activity above 100 km.

1. Introduction

Atmospheric large-scale waves, for example, planetary waves (PWs), play significant roles in the middle and upper atmosphere dynamics, contributing to energy transport between atmospheric levels (e.g., Holton, 1975). The impetuous development of numerical technologies contributes to the evolution of models of general atmospheric circulation, which are increasingly capable of more and more accurate descriptions of various aspects of atmospheric motions. This leads to increasing interest in detailed understanding of the dynamical and thermal effects made by atmospheric waves of different scales. Nowadays, numerous studies are devoted to modeling the different effects of wave interactions in the atmosphere (e.g., Becker & Vadas, 2018; Chang et al., 2014; Liu et al., 2004; Wang et al., 2017).

Solar activity (SA) experiences cyclic variations with the period of about 11 years (e.g., Hathaway, 2010), affecting thermal and dynamical features of the atmospheric circulation. It leads to significant changes in the propagation of PWs at different atmospheric layers (Arnold & Robinson, 1998; Geller & Alpert, 1980; Koval et al., 2018a; Liu & Richmond, 2013). SA effects may influence the PW propagation and reflection conditions in the middle atmosphere. This was confirmed by Chanin (2006), who compared data of 45-year measurements of the thermal structure of the middle atmosphere with numerical simulations. Krivolutsky et al. (2015) also investigated SA effects using numerical modeling. Analyses of the long-term wind measurements in the region of mesosphere and lower thermosphere showed correlations between PW activity and solar radio flux $F_{10.7}$ (Jacobi et al., 2008). Significant changes of the PW activity were disclosed when analyzing

the responses of the annual mean temperature and its seasonal variations to the solar 11-year cycle (Gan et al., 2017). Partial reflection of PWs propagating from the troposphere to the lower thermosphere could also affect the middle atmosphere circulation (e.g., Lu et al., 2017). Changes in conditions of PW reflection at mesosphere and lower thermosphere altitudes may be connected with considerable changes in wind and temperature gradients at different SA levels (e.g., Koval et al., 2018b). Amid other factors influencing the PW propagation to the thermosphere, the stratospheric sudden warming events (e.g., Cullens et al., 2015) could be mentioned.

The middle and upper atmosphere model (MUAM) was extended to simulate the general circulation and PWs at heights from the troposphere up to 300–400 km (Pogoreltsev et al., 2007). Simulations with the MUAM by Koval et al. (2018a, 2018b) revealed substantial changes in general circulation and PWs at heights above 100 km due to SA variations. Below 100 km, the results of simulations by Koval et al. (2018a, 2018b) have no sufficient statistical confidence and do not allow making reliable conclusions about SA influence on dynamics of the middle atmosphere.

In this study, we extended the number of MUAM runs and obtained statistically confident results showing substantial response of the upper stratospheric and mesospheric dynamics to SA changes at heights above 100 km. Simulations with the MUAM were performed at altitudes 0–300 km with inclusion of SA effects corresponding to different SA at altitudes above 100 km. In this way, we avoid the direct solar radiation impacts on the middle atmosphere (e.g., Kodera & Kuroda, 2002) and purified possible dynamical coupling of the thermosphere and the middle atmosphere through PW-mean flow interactions. The most interesting conclusion is that impacts of SA changes on the thermosphere above 100 km can significantly influence the mean wind, temperature, and PW amplitudes at altitudes below 100 km, which was, for the first time, confirmed at significance level of 95%. These results of simulations for extended number of the MUAM runs are essential for further understanding of mechanisms of SA impacts on the dynamics of the middle atmosphere. We have not found such statistically confident simulations in the literature.

2. Numerical Model and Methodology

To obtain changes in the global circulation and PW parameters in the middle atmosphere, numerical simulations with the nonlinear mechanistic MUAM model (Pogoreltsev, 2007; Pogoreltsev et al., 2007) were performed. This model is developed on the basis of the finite differences Cologne Model of the Middle Atmosphere-Leipzig Institute for Meteorology (COMMA-LIM) described by Fröhlich et al. (2003). The key characteristics and physical processes involved in the model were discussed by Gavrilov et al. (2005) and by Koval et al. (2018a). In particular, the MUAM includes a parameterization of thermal and dynamical effects produced by a spectrum of nonorographic internal gravity waves (GWs; e.g., Gavrilov, 1997) and of mountain waves (Gavrilov & Koval, 2013). Horizontal grid of the MUAM involves 64×36 nodes in longitude and latitude, respectively. In the current MUAM version, the log-isobaric vertical grid has 56 levels spanning heights from the ground to 300 km. The simulation in time has the step of 225 s. PW amplitudes near the ground are set using distributions of geopotential height taken from the 55-year Japanese reanalysis data set (Kobayashi et al., 2015) averaged over years 2005–2014 for January.

The MUAM includes standard radiation schemes (Fröhlich et al., 2003) for the rates of solar heating and infrared cooling due to the main absorbing and emitting atmospheric gas species. Also, the model accounts for turbulent and molecular viscosity and thermal conduction, as well as ion drag. In the thermosphere, the MUAM includes an extended parameterization of ultraviolet heating with fluxes of solar radiation and absorption coefficients for different gas species and different spectral intervals taken from the model by Richards et al. (1994).

The MUAM includes thermal and dynamical GW effects, which are necessary for proper simulations of the general circulation in the upper and middle atmosphere (Andrews et al., 1987). Such GWs have subgrid scales and should be parameterized. The MUAM involves different GW parameterizations (Zarubin & Pogoreltsev, 2014). For GWs with phase speeds of 5–30 m/s, a Lindzen-type parameterization (Lindzen, 1981) is used. For GWs having phase speeds of 30–125 m/s, which are important in the thermosphere, the MUAM includes a kind of spectral parameterization (Yigit & Medvedev, 2009). It uses 15 spectral wave components having periods between 40 min and 3 hr. The MUAM includes also a parameterization of stationary orographic GWs (Gavrilov & Koval, 2013).

The stages of obtaining steady-state MUAM solutions from initial windless conditions include maintaining constant geopotential heights at the ground in 30 beginning model days and triggering the heating daily variations starting from the 120th day. After the 300th day, seasonal variations of solar heating are included. Test simulations performed by Pogoreltsev et al. (2007) revealed that stages described above allow the model to reach a steady-state condition by the 300th day. Therefore, the 301st–390th days are considered as characteristic for December–February.

As an indicator of different SA levels, the MUAM radiation block uses the solar flux of radio waves with the 10.7 cm wavelength ($F_{10.7}$). The $F_{10.7}$ flux is cyclically changed with periods about 11 years (Tapping, 1987). These changes correlate with changes in the Wolf number; therefore, the $F_{10.7}$ flux is a common SA characteristic. Based on the measurements throughout six last solar cycles in the Royal Observatory of Belgium (ROB) (2013), Koval et al. (2018a, 2018b) chose the values of $F_{10.7}$ = 220, 130, 70 sfu for the high, medium, and low SA levels, respectively (1 sfu = 10^{-22} W/(m^2 Hz)).

As far as the main goal of this paper is considering thermospheric effects of SA variations, minimum and maximum values of $F_{10.7}$ were specified at heights above 100 km. Below 100 km, the same value of $F_{10.7}$ = 130 sfu (matching to the medium SA) was specified in all MUAM runs. To account for the impact of ionized components on the neutral gas movement for different SA, ionospheric conductivities and their temporal, longitudinal, and latitudinal inhomogeneities (Shevchuk et al., 2018) were involved into the MUAM (see Koval et al., 2018b). Ion drag and geomagnetic torque were calculated taking parameters from the IRI-Plus ionospheric model (Gulyaeva et al., 2002) and from the NRL-MSISE model of the neutral atmosphere (Picone et al., 2002). They were implemented into the MUAM at 23 nodes of vertical grid above 100 km taking into account diurnal variations.

To interpret the simulated PW characteristics of all analyzed PW modes, the altitude-latitude distributions of the quasi-geostrophic zonal-mean refractivity index squared (RI^2) were calculated (e.g., Albers et al., 2013). According to PW theory, regions of positive RI^2 values can be considered as waveguides, within which PWs can propagate. In regions of a negative RI^2, the waves should be attenuated (e.g., Dickinson, 1968; Matsuno, 1970). For further diagnostics of PW propagation, the Eliassen-Palm (EP) flux was calculated (e.g., Andrews et al., 1987). The EP flux directed upward corresponds to the PW heat flux directed to the north, although the southward EP flux corresponds to the northward wave momentum flux. Used formulas were discussed by Gavrilov, Koval, et al. (2018). In addition, EP flux divergence was calculated, which determines the acceleration of zonal-mean stream produced by PWs (Andrews et al., 1987).

To achieve sufficient statistical confidence, 16 pairs of the model runs for low and high SA were performed. The background conditions in all MUAM runs were the same. However, the dynamics of the atmosphere is sensitive to the phases of vacillations between PWs and the mean wind in the stratosphere and to variations of initial conditions (e.g., Gray et al., 2003; Yoden, 1990). Initial perturbations together with PW phases depend on the model day of inclusion of daily variations of solar heating mentioned above in the course of the MUAM initialization, which varies between 120 and 135 with the step of 1 day in the simulated ensemble of 16 pairs of the MUAM runs. From each MUAM run, the same temporal interval between the middle of December and the end of February was extracted. For calculating the mean global circulation and PW characteristics, this interval was divided into five 15-day subintervals. For each subinterval, amplitudes and phases of PW modes having zonal wavenumbers m = 1–4 at zero frequencies were estimated using Fourier transform with the least squares fitting longitude-time structure of hydrodynamic fields. In the present study, we call these PWs the conventional term "stationary planetary waves" (SPWs). SPW with zonal wavenumbers m = 1–4 are designated as SPW1–4 thereafter. To estimate SA influences, for each of 16 pairs of the MUAM runs for high and low SA, the differences between the temperature, mean wind, and SPW amplitude at each grid point were obtained and averaged over altitude-latitude cluster containing nine adjacent grid points. This gives 720 individual differences (16 runs * 5 subintervals * 9 grid points) for usage of the Student's paired t test (e.g., Rice, 2006). This methodology let us get statistically confident differences at 95% significance level between the mean values of SPW amplitudes under high and low SA at almost all heights below 100 km.

3. Results of Simulations

To investigate the thermospheric SA impact on the middle atmosphere circulation and SPWs, we analyzed sets of 720 differences in the atmospheric parameters and in amplitudes of SPWs between respective pairs of

model runs in the vicinity of each grid point at low and high SA levels extracted from eighty 15-day subintervals (see section 2). Besides improving statistical confidence, this approach allowed us to smooth out influences of intense dynamical perturbations, for example, stratospheric sudden warming events arising in individual model runs.

3.1. Changes in SPW Amplitudes

Amplitudes of SPWs at each latitude and altitude were obtained for all eighty 15-day subintervals using least squares fit of longitude dependence of hydrodynamic fields with sinusoidal components having different zonal wavenumbers m at zero frequency. According to properties of the Fourier transform at limited time intervals, obtained amplitudes contain actual contributions from PWs with periods longer than 15 days. Geopotential height amplitudes of the SPW modes with $m = 1$–4 for the high SA level averaged over eighty 15-day subintervals are shown in the left panels of Figures 1 and 2 for geopotential altitude ranges 0–300 and 0–100 km, respectively. Structures and magnitudes of simulated SPW amplitudes in Figures 1 and 2 are in general agreement with satellite measurements (e.g., Forbes et al., 2002; Mukhtarov et al., 2010; Xiao et al., 2009) and with our previous simulations (Koval et al., 2018b).

Corresponding RI^2 and EP fluxes for SPW modes with $m = 1$–4 for high SA at altitudes 0–100 km are represented in the left panels of Figure 3. At heights 30–60 km, waveguides with $RI^2 > 0$ exist in the winter (northern) hemisphere, where the mean zonal wind is eastward (see the left panel of Figure 5a). In the summer (southern) hemisphere, the mean zonal wind is directed to the west at altitudes 30–60 km, and regions with $RI^2 < 0$ prevent upward PW propagation from below. This may explain why SPW amplitudes at altitudes 30–60 km are maximum in the winter (northern) hemisphere in the left panels of Figures 1 and 2.

According to recent views, SPWs might be generated in the lower atmosphere. In winter, they can propagate upward-southward along the waveguides with positive RI^2 represented in the left panels of Figure 3. Therefore, EP flux vectors are directed mostly upward and southward in the northern middle atmosphere at altitudes below 80–90 km. At altitudes above 60 km, the mean zonal wind become eastward in the summer hemisphere (see Figure 5a), and waveguides with $RI^2 > 0$ span both hemispheres in the left panels of Figure 3. Therefore, SPW modes can penetrate into the Southern Hemisphere, and amplitudes of all SPW modes become comparable in both hemispheres at altitudes above 100 km (see the left panels of Figure 1). SPW1 mode has the largest amplitudes at latitudes 60–70°N and heights 50–60 km in the left panel of Figure 2a. SPW waveguides for larger zonal wavenumber in the lower left panels of Figure 3 become narrower and are shifted toward lower latitudes in the Northern Hemisphere. Accordingly, the amplitude maxima of SPW modes having larger m in the left lower panels of Figures 2c and 2d are located at lower latitudes compared to Figure 2a.

Changes in the thermospheric parameters produced by SA impacts can modify configurations of the SPW waveguides and, hence, can change their spatial structures and amplitudes. Average differences in the SPW amplitudes for high and low SA are depicted in the right panels of Figures 1 and 2. These differences are relatively small and require statistical verifications. Numerical experiments showed that sufficient statistical confidence could be obtained only for the differences averaged over nine nearby nodes of the MUAM altitude-latitude grid. In this case we have 720 pairs of simulated amplitudes (16 MUAM runs * 5 time subintervals * 9 nearby grid nodes) in the vicinity of each grid node. Regions, where paired Student's t tests gave the probabilities of nonzero differences at significance level $\alpha > 95\%$, are hatched with horizontal lines in the right panels of Figures 1 and 2. One could notice that obtained differences in SPW amplitudes for high and low SA are statistically reliable in almost all altitude-latitude regions.

In the right panels of Figure 1, the differences at geopotential heights above 100 km are similar to those obtained and discussed in our previous study (Koval et al., 2018a) and are caused by modifications of the thermospheric mean temperature and wind by changing SA (see section 3.2). The right panels of Figure 2 reveal that SA impacts in the thermosphere can also make modifications of SPW amplitudes at altitudes below 100 km. Magnitudes of the differences in the right panels of Figure 2 can reach up to 10–15% of the peak values in the respective left panels of Figure 2 in the northern middle atmosphere depending on wavenumber. At high and middle latitudes of the Northern Hemisphere, SPW1 amplitudes at heights below 40–50 km are commonly larger at high SA. Between heights 50–70 km at high northern latitudes, SPW1

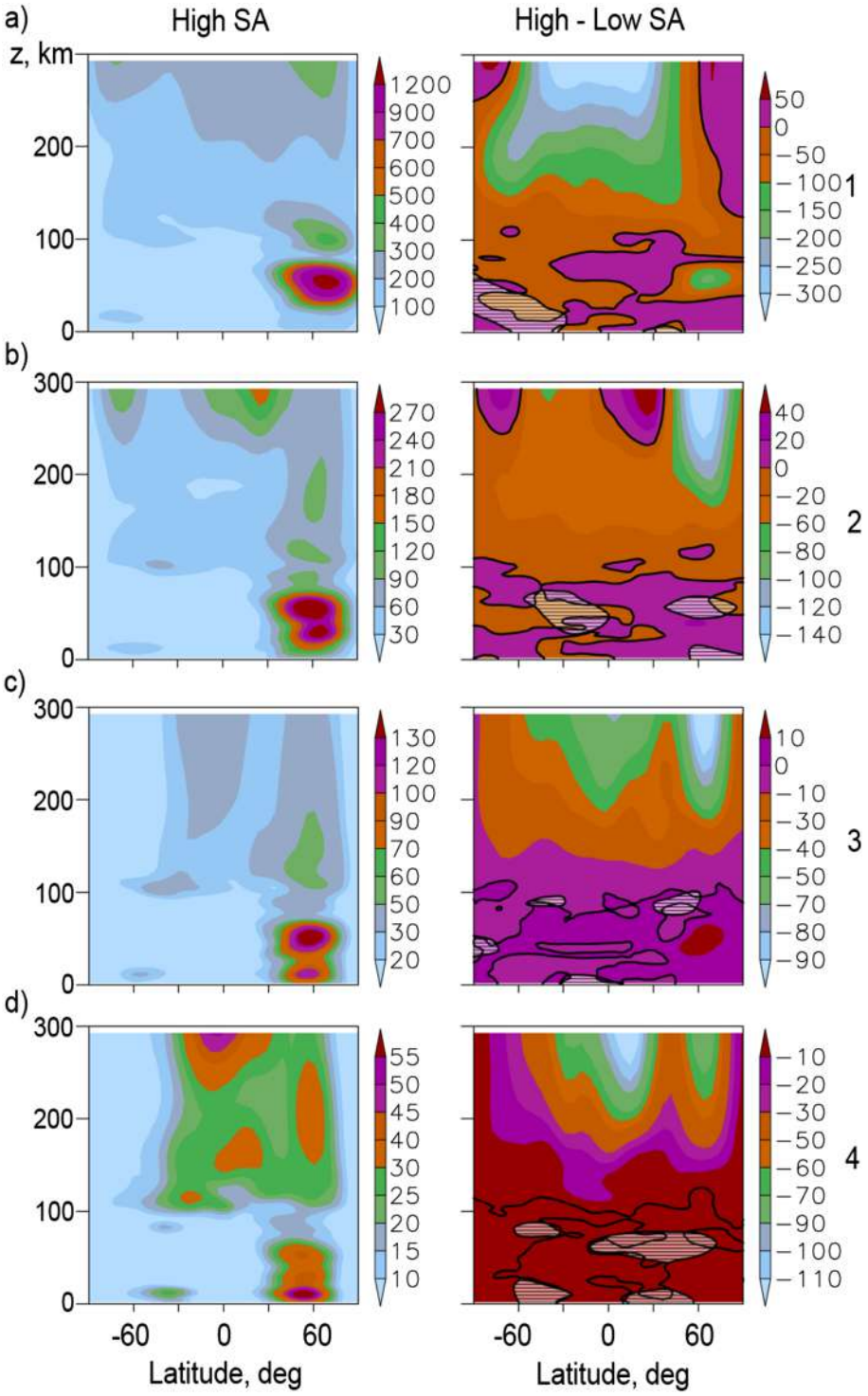

Figure 1. Altitude-latitude distributions of geopotential height amplitudes (in geopotential meters) at high SA (left) and their differences from those at low SA (right) for SPW modes with zonal wavenumbers $m = 1$–4 (a–d, respectively) averaged for eighty 15-day intervals taken from 16 pairs of the MUAM runs. Solid lines show zero levels. Hatched areas indicate regions, where the nonzero differences have statistical confidence less than 95% according to the paired t test.

amplitudes are smaller at high SA in the right panel of Figure 2a. For SPW2–SPW4 modes in the right panels of Figures 2b–2d the regions of negative differences at altitudes 50–80 km are smaller than those for SPW1 mode in the right panel of Figure 2a.

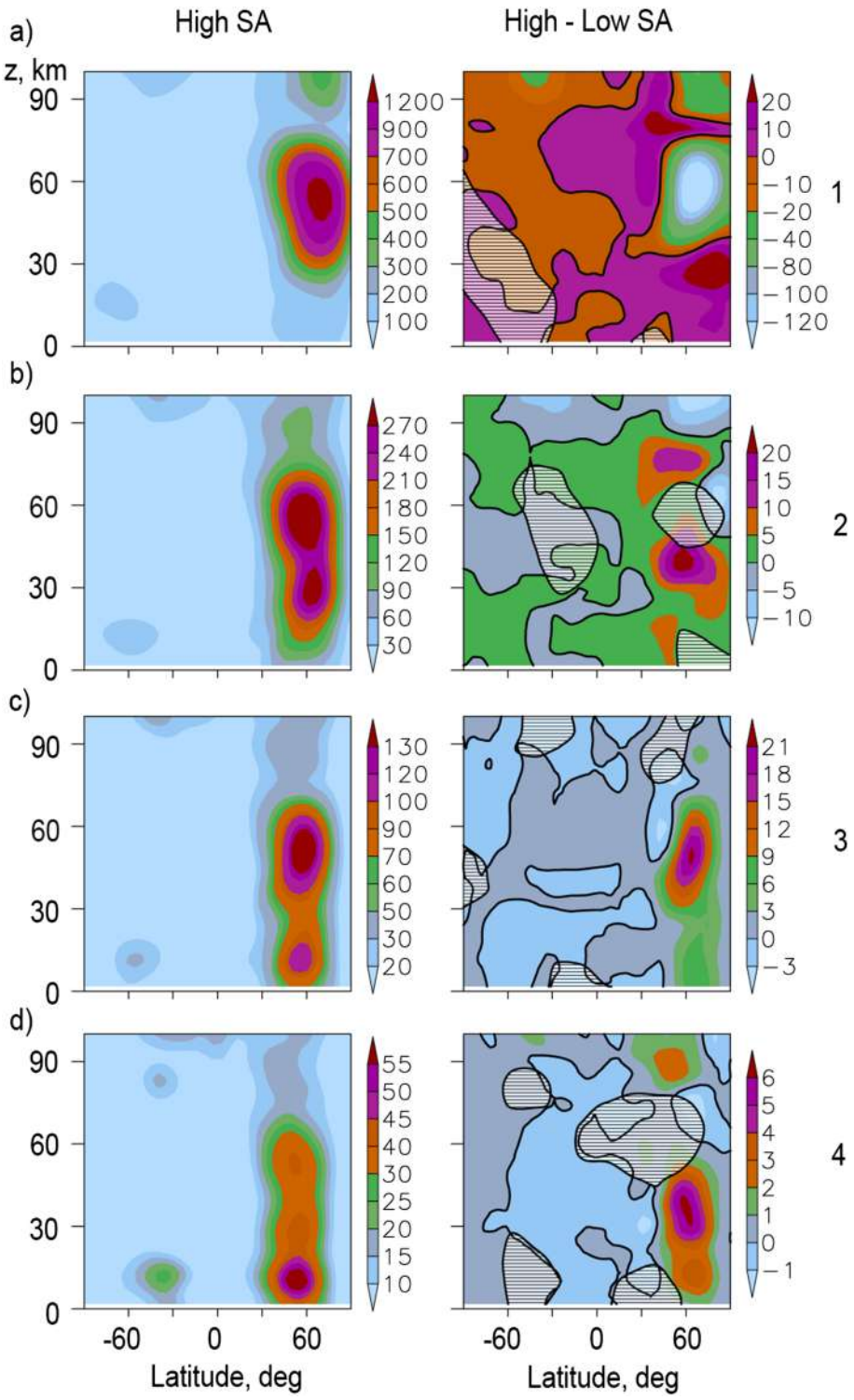

Figure 2. The same as Figure 1, but for altitudes 0–100 km.

In Figure 2, the main changes in SPW amplitudes match with variations of respective EP fluxes in Figure 3. Northward and downward directed vectors of EP flux differences in the right panels of Figure 3 are opposite to the main directions of respective EP fluxes of SPW modes in the left panels of Figure 3 and may reflect modifications in SPW propagation conditions at different SA levels. This can explain negative values of

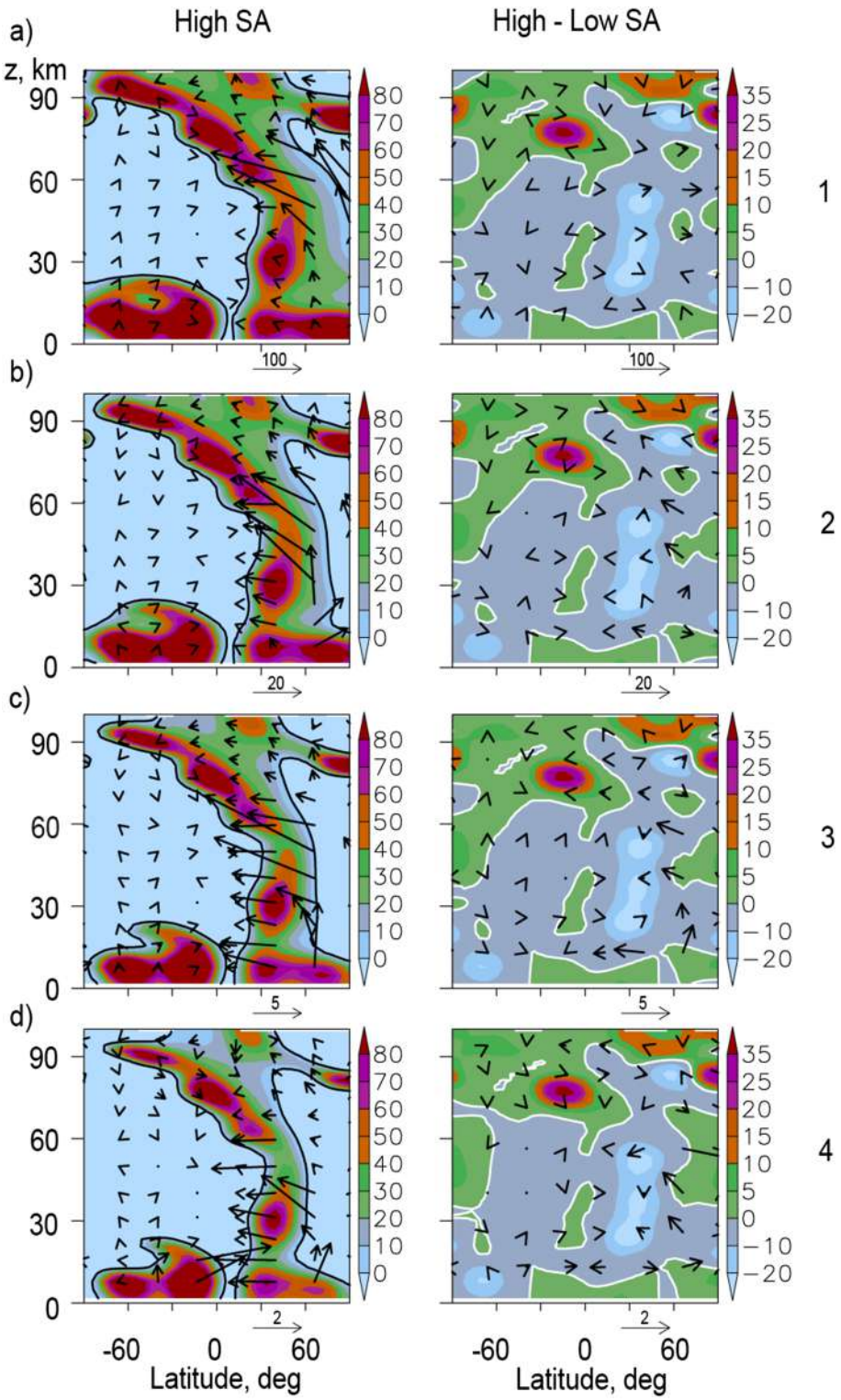

Figure 3. Normalized refractivity index squared (shaded) and vectors of the EP flux in 10^{-2} m^3/s^2 (arrows) for SPW having m = 1–4 (a–d, respectively) at high SA (left), also their differences from those at low SA (right). Solid lines show zero levels.

differences in the SPW amplitudes within the respective regions of the right panels of Figure 2. Positive SPW amplitude differences in the right panels of Figure 2 generally correspond to the southward and upward directions of the vectors differences of EP flux in the right panels of Figure 3.

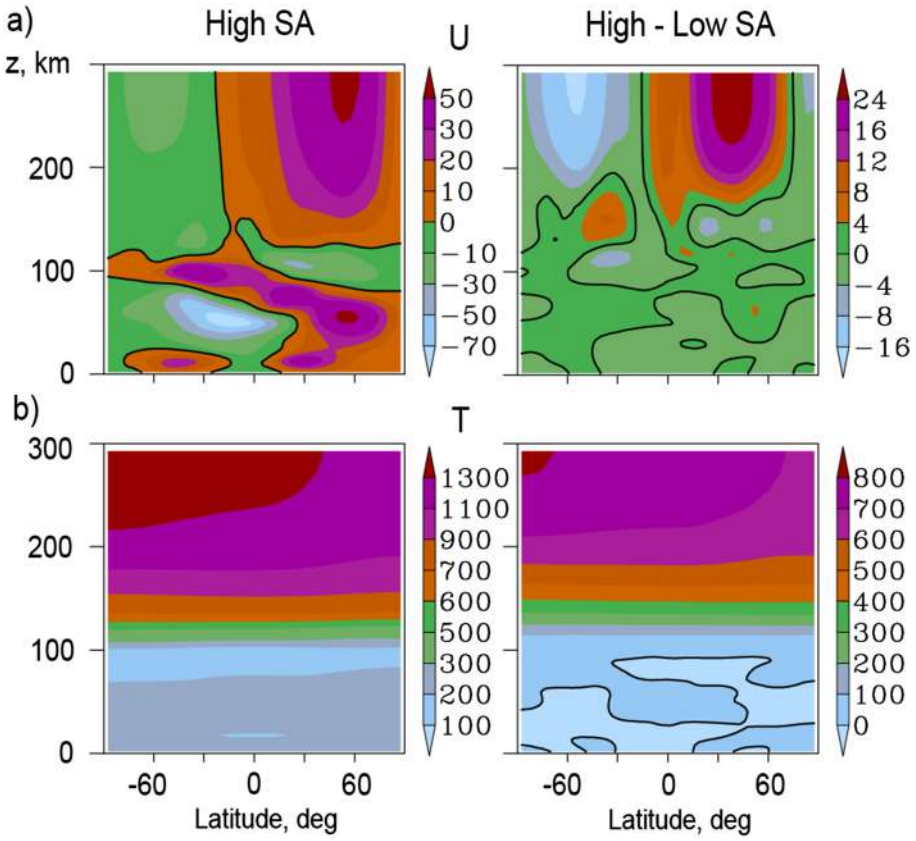

Figure 4. Altitude-latitude distributions of the mean zonal wind in m/s (a, left) and temperature in K (b, left) at high SA, also their differences from the low SA (right panels) in middle December–February averaged for 16 MUAM runs. Solid lines show zero levels.

Besides RI^2 and EP flux structures, significant influence on SPWs propagating from below may have their partial reflection at the lower thermosphere heights (e.g., Lu et al., 2017). For example, negative values of the SPW1 amplitude differences at high and middle northern latitudes and altitudes 40–80 km in the right panel of Figure 2a are accompanied by their positive differences at heights above 100 km in the respective right panel of Figure 1a. For SPW2–SPW4 modes, negative amplitude differences at high northern latitudes at heights above 100 km in the right panels of Figures 1b–1d correspond to positive differences in their amplitudes at high northern latitudes at altitudes below 100 km in the right panels of Figures 2b–2d. This behavior can be explained by better reflection of SPW2–SPW4 modes compared to SPW1 at high SA in the lower thermosphere.

Substantial impacts on SPW amplitudes may come from wave-mean flow and wave-wave nonlinear interactions. For instance, SPWs can be generated in the atmosphere beyond the waveguides shown in the left panels Figure 3, where many EP flux vectors are originated in the regions with negative RI^2.

3.2. Changes in the Zonal Circulation

The left panels of Figures 4a and 4b show, respectively, latitude-altitude dependences of the mean temperature and zonal wind at geopotential heights 0–300 km averaged over the interval from the middle December–February and over 16 MUAM runs at high SA. At altitudes below 100 km, they correspond to semiempirical models of temperature (Picone et al., 2002) and zonal wind (e.g., Drob et al., 2008; Jacobi et al., 2009). The right panels of Figures 4a and 4b show respective differences between high and low SA impacts in the thermosphere. The right panel of Figure 4b shows the mean temperature differences, which can reach up to 800 K. The MUAM contains the hydrostatic equation and the state equation of ideal gas, which relate atmospheric pressure and density with temperature. Therefore, temperature changes shown in

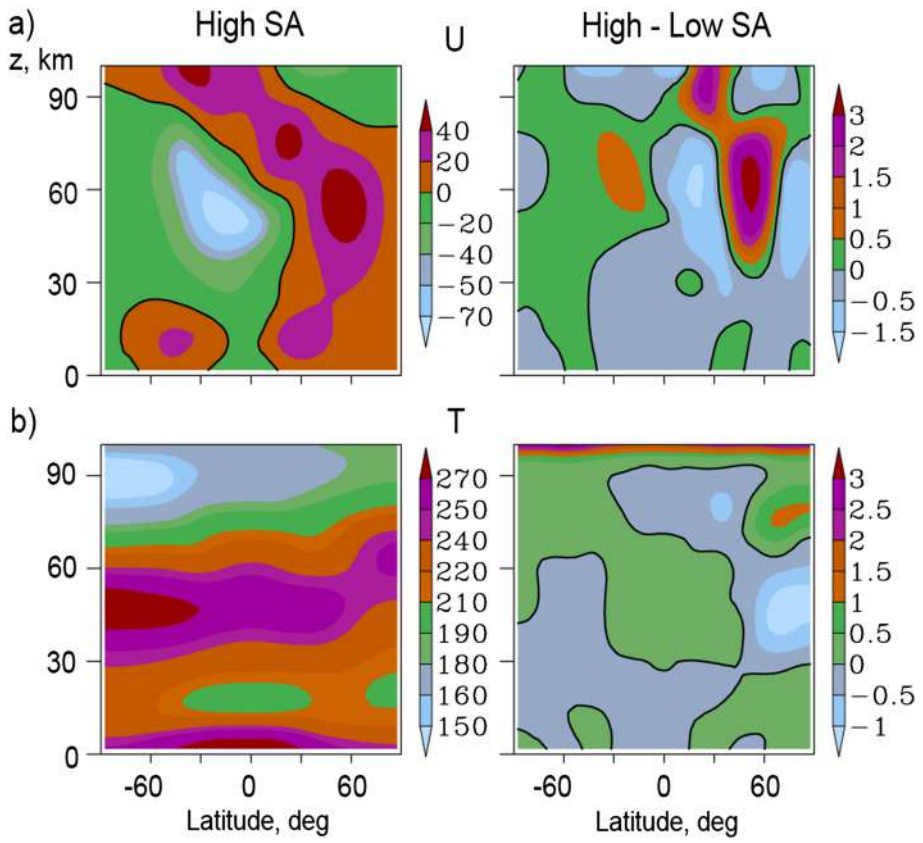

Figure 5. The same as Figure 4, but for altitudes 0–100 km.

Figure 4b give respective changes in atmospheric pressure and density. Our analysis revealed that variations of temperature, pressure, and density simulated with the MUAM match to the MSISE standard atmosphere model.

The right panel of Figure 4a shows that magnitudes of the mean zonal wind are stronger (up to 50%) at altitudes higher than 180 km and weaker at 140–180 km at high SA level in both hemispheres. Koval et al. (2018b) interpreted this behavior to be associated with solar flux influence on meridional temperature gradients. For example, in the Northern Hemisphere, increasing northward temperature gradient between 140 and 180 km at high SA corresponds to decrease in the eastward wind speed and to negative wind differences in the right panel of Figure 4a. This corresponds to classical theory of "the thermal wind" (e.g., Gill, 1982).

Figure 5 reproduces Figure 4 but for the altitude range 0–100 km. For estimating the statistical confidence of the differences showed in the right panels of Figures 4 and 5, the paired Student's t test was used. For the respective pairs of the MUAM runs under low and high SA at every latitude-altitude grid point there are 921,600 pairs of wind components and temperature values (16 model runs * 900 two-hour outputs * 64 longitude nodes). At significance level $\alpha = 95\%$ the mean differences in temperature and zonal wind are satisfied to the hypothesis of their nonzero values at all grid points in the right panels of Figures 4 and 5.

The right panels of Figure 5 reveal that the mean differences of the zonal wind and temperature due to thermospheric SA impacts are smaller at heights below 100 km than those above 100 km in Figure 4. They can reach 3–4 m/s and 3 K at altitudes 40–100 km at high northern latitudes. This illustrates that variations of thermospheric parameters at heights above 100 km due to SA variations can influence the mean flow in the middle atmosphere as well. At heights 40–100 km, average temperature differences have maximum magnitudes at high and middle latitudes of the Northern Hemisphere in the right panel of Figure 5b. The mean wind and temperature differences are smaller at altitudes 30–60 km of the summer (southern) hemisphere, where $RI^2 < 0$ and SPW propagation from below is suppressed (see Figure 3)

Other researchers reported changes of the mean zonal wind and temperature in the middle atmosphere due to SA changes. Analyzing the regression coefficients between SA and the mean temperature and zonal wind in winter months based on the European Centre for Medium-Range Weather Forecasts Reanalysis-Interim atmospheric reanalysis data showed noticeable changing in these fields at altitudes up to 60 km (Crooks & Gray, 2005) and at pressure levels below 1 hPa (Kodera et al., 2016). In particular, Crooks and Gray (2005) have reported statistically reliable heating in the tropical and cooling in the extratropical stratosphere under conditions of solar maximum in the data of European Centre for Medium-Range Weather Forecasts Reanalysis-40. Arnold and Robinson (2003) made simulations of SA and GW impacts on atmospheric circulation for boreal winters and obtained general structure of the differences in the mean temperature and zonal wind analogous to our right panels of Figures 4 and 5. Using the chemistry-climate model SOCOL, Rozanov et al. (2008) performed numerical simulations to estimate solar irradiance influence on general atmospheric circulation. The results they obtained for the northern winter conditions are in general agreement with the results described above. These simulations did not involve thermospheric heights and considered changes of general circulation due to changes in radiation balance, GW activity, and photochemistry within the middle atmosphere at different SA levels. In our simulations, we kept radiation balance and composition below 100 km unchanged at all SA levels. Therefore, it is thoughtless to make point-by-point comparisons of Figures 4 and 5 with studies mentioned above. However, our simulations show that modifications of atmospheric parameters at heights above 100 km caused by SA may produce effects in the middle atmosphere comparable with impacts of changes in solar radiation and photochemistry at altitudes below 100 km.

In order to recognize the reasons of the zonal wind and temperature differences in the middle atmosphere due to SA thermospheric impacts in our study, we analyzed different terms in MUAM equations of motion and heat balance at heights below 100 km. The main distinctions were found in the heat influxes caused by the horizontal advection of heat and by diabatic heating/cooling due to vertical air motions at high northern latitudes. Such heating/cooling differences (dynamical in nature) might be caused by interactions between the mean flow and PWs propagating from the lower layers of the atmosphere. Figure 6 represents the EP flux vertical component for SPW1 (which is much stronger than other SPW modes) and the EP flux divergence calculated for winter months. The left and right panels of Figure 6 reveal discussed quantities at high SA level and respective differences between high and low SA.

Theory of atmospheric PWs (e.g., Andrews et al., 1987) shows that upward directed EP flux matches with the wave heat flux directed to the north and, hence, to warming of the middle atmosphere at high latitudes. Figure 6a shows that SA influence in the thermosphere can modify conditions of PW propagation and reflection and can produce changes in EP fluxes in the middle atmosphere as well. The right panel of Figure 6a at high northern latitudes shows negative differences in the EP flux at altitudes 30–60 km and generally positive differences above 60 km, which corresponds very well to negative and positive temperature differences in respective altitude layers in the right panel of Figure 5b. Such heating/cooling of the high latitude middle atmosphere can modify meridional temperature gradients and influence the mean zonal wind in respective atmospheric layers. Additional impacts may exert accelerations of zonal wind produced by PWs and depending on the EP flux divergence (e.g., Andrews et al., 1987). The right panel of Figure 6b shows maxima and minima of the differences in SPW1 EP flux divergence at altitudes 40–100 km, at middle and high northern latitudes, where the right panel of Figure 5a shows substantial zonal wind differences.

Section 3.1 shows that modifications of the mean wind and temperature may change conditions of wave propagation in the atmosphere leading to variations of SPW characteristics. On the other hand, changes in SPW EP flux components may exert wave accelerations and heat influxes producing modifications of the mean atmospheric circulation and temperature. Therefore, interactions between the middle atmosphere circulation and SPWs is not a stationary process but produce so-called “vacillations” having periods up to several weeks (e.g., Holton & Mass, 1976). The results of the MUAM simulations also contain such vacillations (e.g., Gavrilov, Koval, et al., 2018). Hence, the mean circulation and SPW characteristics discussed above reflect cumulative effects of these vacillations averaged over the winter season.

In the right panels of Figures 5 and 6, differences of all quantities at high and low SA are stronger within the Northern Hemisphere compared to those in the southern (summer) one, where zonal wind reversal at about 20 km prevent direct SPW propagation from the lower atmosphere (e.g., Charney & Drazin, 1961). This

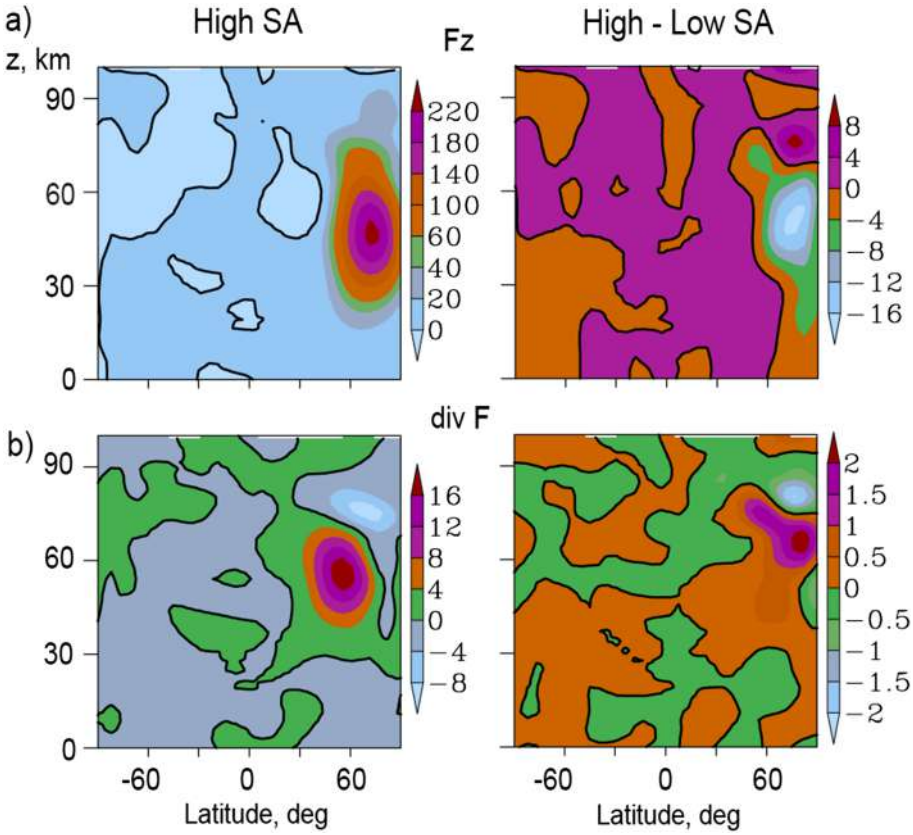

Figure 6. SPW1 vertical EP flux component in 10^{-2} m^3/s^2 (a, left) and EP flux divergence in m/s/day (b, left) for high SA and their respective differences from the low SA (right panels) in middle December–February averaged for 16 MUAM runs. Solid lines show zero levels.

confirms that changes in SPW propagation and reflection conditions at thermospheric altitudes can modify SPW characteristics, wave-mean flow interactions, thermal regime, and general circulation in the middle atmosphere in winter season. Statistically confident nonzero differences of the SPW amplitudes, mean zonal wind, and temperature at heights below 100 km in the right panels of Figures 2 and 5 give confirmations that modifications of thermospheric characteristics due to SA influence can affect the middle atmosphere circulation and SPW characteristics at heights below 100 km.

One of the other reasons for the mean wind and temperature changes in the atmosphere could be dynamical and thermal effects of GWs. Numerous studies show dependences of GW characteristics on SA in the thermosphere (e.g., Klausner et al., 2009; Yigit & Medvedev, 2010). SA affects thermospheric temperature, density, dissipation, and static stability, which can influence GW propagation conditions (e.g., Vadas & Fritts, 2006). Simulations with a high-resolution nonlinear GW model showed that resulting GW dynamical effects at any thermospheric height at increased SA depend on increase in the wave amplitudes because of smaller molecular viscosity and smaller transfer of wave energy to the mean wind and on decrease in the amplitudes due to larger density and larger wave reflection (Gavrilov, Kshevetskii, & Koval, 2018). Analyzing the wave drag and heat influxes made by GW parameterizations in the MUAM indicated their substantial values at altitudes above 80–100 km. SA variations produce changes of GW drag and heat influxes in the thermosphere similar to those reported by Yigit and Medvedev (2010). These changes may modify the mean temperature, wind, and SPW waveguides, especially in the lower thermosphere. Differences in the mean wind and temperature for high and low SA in the right panels of Figure 5 exist at altitudes below 80–100 km, where GW drag and heat influxes are smaller than those produced by SPWs. Therefore, in the MUAM the main GW impacts at different SA provide changes in the mean wind and temperature in the thermosphere, which vary reflection conditions for SPWs propagating from the lower atmosphere and change their dynamical and thermal features.

In addition to changes in SPW propagation and reflection conditions discussed above, variable SA can produce substantial changes in thermospheric pressure, temperature, density, molecular viscosity, and heat conduction (see, e.g., Figure 1 of the paper by Gavrilov, Kshevetskii, & Koval, 2018). These changes can help for penetration of thermospheric perturbations to the middle atmosphere. Major differences in the mean wind and temperature in the right panels of Figure 5 are generally located along the SPW waveguides in the left panels of Figure 3. In addition, the differences are smaller at altitudes 30–60 km of the Southern Hemisphere, where upward SPW propagation is suppressed. This gives evidences that changes in SPW propagation and reflection conditions due to variable SA dominates over direct influences of thermospheric impacts on the middle atmosphere mentioned above. However, further studies of different mechanisms of influence of thermospheric processes on the lower atmospheric layers are required.

Some studies (e.g., Kodera & Kuroda, 2002) showed that changes in ultraviolet radiation during solar cycle might influence the mean temperature and wind, as well as PW propagation conditions and EP flux components in the stratosphere. Our results reveal noticeable impacts on these characteristics in the mesosphere from thermospheric variations due to changing solar activity. Complete considerations of solar activity influences of the middle atmosphere dynamics require developments of whole atmosphere circulation models accounting for SA impacts at all altitudes.

4. Conclusions

The focus of this paper is on increasing of statistical confidence of numerical simulations of the effect of thermospheric SA impacts on the mean flow and characteristics of SPWs in the middle atmosphere. Two 16-member sets of numerical modeling of atmospheric general circulation for low and high SA were obtained using the three-dimensional mechanistic general circulation model MUAM, which covers altitudes from 0 to about 300 km. The radiation block of the MUAM uses solar flux of radio waves at 10.7 cm as an indicator of different SA levels. Ionospheric conductivities with their latitudinal, longitudinal, and time variations for different SA conditions were involved in the MUAM above 100 km. Amplitudes of SPWs at each latitude and altitude were obtained for each of 15-day subintervals using least squares fit of longitude dependence of hydrodynamic fields with sinusoidal components having different zonal wavenumbers m at zero frequency. Selecting five 15-day subintervals from each of 16 MUAM runs for middle December–February allowed us to obtain 80 pairs of SPW amplitudes with zonal wavenumbers $m = 1$–4. This approach allowed us to achieve statistically confident nonzero differences in SPW amplitude estimations at 95% significance level.

In the thermosphere, changing from the low to high SA level in the MUAM above 100 km enhances magnitudes of zonal wind (up to 50%) at heights above 180 km and weaken them at 140–180 km. This could be associated with SA influence on meridional temperature gradients. At altitudes less than 100 km, differences in SPW amplitudes between high and low SA reach up to 10–15% at middle and high northern latitudes. SPWs propagate upward within waveguides depending on refractivity index squared. Changes in the amplitudes of SPW modes correspond to respective changes in their EP flux components. A significant influence on SPWs propagating from below is their partial reflection at heights of the lower thermosphere. This means that SA impacts at altitudes above 100 km may change proportions of reflected SPW energy, which can modify dynamics and temperature at heights below 100 km.

Differences of the mean zonal wind and temperature for high and low SA impacts can reach 10% at altitudes 40–100 km at high and middle northern latitudes. The major distinctions were detected in the MUAM heat balance equation containing heat influxes due to the horizontal advection of heat and diabatic heating/cooling due to vertical air motions at high northern latitudes. There are substantial increases and decreases of upward EP flux component at heights 40–100 km, which matches with respective increases and decreases in temperature at high northern latitudes under high SA. The nonzero differences in temperature and zonal wind are statistically confident at almost all latitude-altitudinal grids. The general structure of simulated zonal wind and temperature differences due to SA impact coincides with the results of previous numerical simulations and with studies based on the atmospheric reanalysis data. This gives statistically confident confirmations of existing views that variations in the thermosphere due to variable SA may affect the conditions of SPW propagation and reflection, which may produce noticeable dynamical and thermal alterations in the middle atmosphere.

Acknowledgments

Modeling of general circulation and PWs was supported by the Russian Science Foundation (Grant 18-77-00022). The analysis of gravity wave effects at different SA levels was supported by the Russian Basic Research Foundation (Grant 17-05-00458). The data of analyzed modeling are freely accessible online (at https://doi.org/10.5281/zenodo.2567770). In accordance with the Statement 1296 of the Civil Code of the Russian Federation, the Russian State Hydrometeorological University (RSHU) has all rights on the MUAM code. To access and use the computer codes, one should obtain a permission from the Rector of RSHU via the address 79, Voronezhskaya Street, St. Petersburg, Russia, 192007, phone: 007 (812) 372-50-92. The authors can assist in obtaining the permission. In this study, the data obtained in the SPbSU "Geomodel" resource center were used.

References

Albers, J. R., McCormack, J. P., & Nathan, T. R. (2013). Stratospheric ozone and the morphology of the Northern Hemisphere planetary waveguide. *Journal of Geophysical Research: Atmospheres*, *118*, 563–576. https://doi.org/10.1029/2012JD017937

Andrews, D. G., Holton, J. R., & Leovy, C. B. (1987). *Middle atmosphere dynamics* (p. 489). New York: Acad. Press.

Arnold, N. F., & Robinson, T. R. (1998). Solar cycle changes to planetary wave propagation and their influence on the middle atmosphere circulation. *Annales Geophysicae*, *16*(1), 69–76.

Arnold, N. F., & Robinson, T. R. (2003). Solar cycle modulation of the winter stratosphere: The role of atmospheric gravity waves. *Advances in Space Research*, *31*(9), 2121–2126.

Becker, E., & Vadas, S. L. (2018). Secondary gravity waves in the winter mesosphere: Results from a high-resolution global circulation model. *Journal of Geophysical Research: Atmospheres*, *123*, 2605–2627. https://doi.org/10.1002/2017JD027460

Chang, L. C., Yue, L., Wang, W., Wu, Q., & Meier, R. R. (2014). Quasi two day wave-related variability in the background dynamics and composition of the mesosphere/thermosphere and the ionosphere. *Journal of Geophysical Research: Space Physics*, *119*, 4786–4804. https://doi.org/10.1002/2014JA019936

Chanin, M.-L. (2006). Signature of the 11-year cycle in the upper atmosphere. *Space Science Reviews*, *125*(1-4), 261–272. https://doi.org/10.1007/s11214-006-9062-5

Charney, J. G., & Drazin, P. G. (1961). Propagation of planetary-scale disturbances from the lower into the upper atmosphere. *Journal of Geophysical Research*, *66*(1), 83–109. https://doi.org/10.1029/JZ066i001p00083

Crooks, S. A., & Gray, L. G. (2005). Characterization of the 11-year solar signal using a multiple regression analysis of the ERA-40 dataset. *Journal of Climate*, *18*(7), 996–1015. https://doi.org/10.1175/JCLI-3308.1

Cullens, C. Y., England, S. L., & Immel, T. J. (2015). Global responses of gravity waves to planetary waves during stratospheric sudden warming observed by SABER. *Journal of Geophysical Research: Atmospheres*, *120*, 12,018–12,026. https://doi.org/10.1002/2015JD023966

Dickinson, R. E. (1968). Planetary Rossby waves propagating vertically through weak westerly wave guides. *Journal of the Atmospheric Sciences*, *25*(6), 984–1002. https://doi.org/10.1175/1520-0469(1968)025<0984:PRWPVT>2.0.CO;2

Drob, D. P., Emmert, J. T., Crowley, G., Picone, J. M., Shepherd, G. G., Skinner, W., et al. (2008). An empirical model of the Earth's horizontal wind fields: HWM07. *Journal of Geophysical Research*, *113*, A12304. https://doi.org/10.1029/2008JA013668

Forbes, J. M., Zhang, X., Ward, W., & Talaat, E. R. (2002). Climatological features of mesosphere and lower thermosphere stationary planetary waves within ±40 latitude. *Journal of Geophysical Research*, *107*(D17), 4322. https://doi.org/10.1029/2001JD001232

Fröhlich, K., Pogoreltsev, A., & Jacobi, C. (2003). Numerical simulation of tides, Rossby and Kelvin waves with the COMMA-LIM model. *Advances in Space Research*, *32*, 863–868.

Gan, Q., Du, J., Fomichev, V. I., Ward, W. E., Beagley, S. R., Zhang, S., & Yue, J. (2017). Temperature responses to the 11 year solar cycle in the mesosphere from the 31 year (1979–2010) extended Canadian Middle Atmosphere Model simulations and a comparison with the 14 year (2002–2015) TIMED/SABER observations. *Journal of Geophysical Research: Space Physics*, *122*, 4801–4818. https://doi.org/10.1002/2016JA023564

Gavrilov, N. M. (1997). Parameterization of momentum and energy depositions from gravity waves generated by tropospheric hydrodynamic sources. *Annales Geophysicae*, *15*(12), 1570–1580.

Gavrilov, N. M., & Koval, A. V. (2013). Parameterization of mesoscale stationary orographic wave forcing for use in numerical models of atmospheric dynamics. *Izvestiya Atmospheric and Oceanic Physics*, *49*(3), 244–251.

Gavrilov, N. M., Koval, A. V., Pogoreltsev, A. I., & Savenkova, E. N. (2018). Simulating planetary wave propagation to the upper atmosphere during stratospheric warming events at different mountain wave scenarios. *Advances in Space Research*, *61*(7), 1819–1836. https://doi.org/10.1016/j.asr.2017.08.022

Gavrilov, N. M., Kshevetskii, S. P., & Koval, A. V. (2018). Propagation of non-stationary acoustic-gravity waves in thermospheric temperatures corresponding to different solar activity. *Journal of Atmospheric and Solar-Terrestrial Physics*, *172*(3), 100–106. https://doi.org/10.1016/j.jastp.2018.03.021

Gavrilov, N. M., Pogoreltsev, A. I., & Jacobi, C. (2005). Numerical modeling of the effect of latitude-inhomogeneous gravity waves on the circulation of the middle atmosphere. *Izvestia Atmospheric and Oceanic Physics*, *41*(1), 9–18.

Geller, M. A., & Alpert, J. C. (1980). Planetary wave coupling between the troposphere and the middle atmosphere as a possible Sun-weather mechanism. *Journal of the Atmospheric Sciences*, *37*, 1197–1215.

Gill, A. E. (1982). *Atmosphere-ocean dynamics* (p. 662). New York: Academic Press.

Gray, L. J., Sparrow, S., Juckes, M., O'Neill, A., & Andrews, D. G. (2003). Flow regime in the winter stratosphere of the Northern Hemisphere. *Quarterly Journal of the Royal Meteorological Society*, *129*, 925–945.

Gulyaeva, T. L., Huang, X., & Reinisch, B. W. (2002). Ionosphere-plasmasphere model software for ISO. *Acta Geodaetica et Geophysica Hungarica*, *37*(2-3), 143–152.

Hathaway, D. H. (2010). The solar cycle. Living Rev. Solar Phys. 7, 1.

Holton, J. R. (1975). The dynamic meteorology of the stratosphere and mesosphere. *Meteorological Monographs*, *15*(37), 218.

Holton, J. R., & Mass, C. (1976). Stratospheric vacillation cycles. *Journal of the Atmospheric Sciences*, *33*(2218), 2215.

Jacobi, C., Fröhlich, K., & Portnyagin, Y. (2009). Semi-empirical model of middle atmosphere wind from the ground to the lower thermosphere. *Advances in Space Research*, *43*, 239–246.

Jacobi, C., Hoffmann, P., & Kurschner, D. (2008). Trends in MLT region winds and planetary waves, Collm (52°N, 15°E). *Annales Geophysicae*, *26*(5), 1221–1232.

Klausner, V., Fagundes, P. R., Sahai, Y., Wrasse, C. M., Pillat, V. G., & Becker-Guedes, F. (2009). Observations of GW/TID oscillations in the F_2 layer at low latitude during high and low solar activity, geomagnetic quiet and disturbed periods. *Journal of Geophysical Research*, *114*, A02313. https://doi.org/10.1029/2008JA013448

Kobayashi, S., Ota, Y., & Harada, H. (2015). The JRA-55 Reanalysis: General specifications and basic characteristics. *Journal of the Meteorological Society of Japan*, *93*, 5–48. https://doi.org/10.2151/jmsj.2015-00

Kodera, K., & Kuroda, Y. (2002). Dynamical response to the solar cycle. *Journal of Geophysical Research*, *107*(D24), 4749. https://doi.org/10.1029/2002JD002224

Kodera, K., Thiéblemont, R., Yukimoto, S., & Matthes, K. (2016). How can we understand the global distribution of the solar cycle signal on the Earth's surface? *Atmospheric Chemistry and Physics*, *16*, 12925–12944. https://doi.org/10.5194/acp-16-12925-2016

Koval, A. V., Gavrilov, N. M., Pogoreltsev, A. I., & Shevchuk, N. O. (2018a). Influence of solar activity on penetration of traveling planetary-scale waves from the troposphere into the thermosphere. *Journal of Geophysical Research: Space Physics*, *123*, 6888–6903. https://doi.org/10.1029/2018JA025680

Koval, A. V., Gavrilov, N. M., Pogoreltsev, A. I., & Shevchuk, N. O. (2018b). Propagation of stationary planetary waves to the thermosphere at different levels of solar activity. *Journal of Atmospheric and Solar - Terrestrial Physics*, *173*, 140–149. https://doi.org/10.1016/j.jastp.2018.03.012

Krivolutsky, A. A., Cherepanova, L. A., Dement'eva, A. V., Repnev, A. I., & Klyuchnikova, A. V. (2015). Global circulation of the Earth's atmosphere at altitudes from 0 to 135 km simulated with the ARM model. Consideration of the solar activity contribution. *Geomagnetism and Aeronomy*, *55*(6), 780–800.

Lindzen, R. S. (1981). Turbulence and stress owing to gravity wave and tidal breakdown. *Journal of Geophysical Research*, *86*, 9707–9714.

Liu, H. L., & Richmond, A. D. (2013). Attribution of ionospheric vertical plasma drift perturbations to large-scale waves and the difference on solar activity. *Journal of Geophysical Research: Space Physics*, *118*, 2452–2465. https://doi.org/10.1002/jgra.50265

Liu, H. L., Talaat, E. R., Roble, R. G., Lieberman, R. S., Riggin, D. M., & Yee, J. H. (2004). The 6.5-day wave and its seasonal variability in the middle and upper atmosphere. *Journal of Geophysical Research*, *109*, D21112. https://doi.org/10.1029/2004JD004795

Lu, H., Scaife, A. A., Marshall, G. J., Turner, J., & Gray, L. J. (2017). Downward wave reflection as a mechanism for the stratosphere-troposphere response to the 11-year solar cycle. *Journal of Climate*, *30*(N), 2395–2414. https://doi.org/10.1175/JCLI-D-16-0400.1

Matsuno, T. (1970). Vertical propagation of stationary planetary waves in the winter Northern Hemisphere. *Journal of the Atmospheric Sciences*, *27*(6), 871–883.

Mukhtarov, P., Pancheva, D., & Andonov, B. (2010). Climatology of the stationary planetary waves seen in the SABER/TIMED temperatures (2002-2007). *Journal of Geophysical Research*, *115*, A06315. https://doi.org/10.1029/2009JA015156

Picone, J. M., Hedin, A. E., Drob, D. P., & Aikin, A. C. (2002). NRLMSISE-00 empirical model of the atmosphere: Statistical comparisons and scientific issues. *Journal of Geophysical Research*, *107*(A12), 1468. https://doi.org/10.1029/2002JA009430

Pogoreltsev, A. I. (2007). Generation of normal atmospheric modes by stratospheric vacillations. *Izvestiya Atmospheric and Oceanic Physics*, *43*(4), 423–435.

Pogoreltsev, A. I., Vlasov, A. A., Fröhlich, K., & Jacobi, C. (2007). Planetary waves in coupling the lower and upper atmosphere. *Journal of Atmospheric and Solar - Terrestrial Physics*, *69*, 2083–2101. https://doi.org/10.1016/j.jastp.2007.05.014

Rice, J. A. (2006). *Mathematical statistics and data analysis* (3rd ed., p. 603). Pacific Grove: Duxbury Press. ISBN-10: 0534399428

Richards, P. G., Fennelly, J. A., & Torr, D. G. (1994). EUVAC: A solar EUV flux model for aeronomic calculations. *Journal of Geophysical Research*, *99*(A5), 8981–8992. https://doi.org/10.1029/94JA00518

Royal Observatory of Belgium (ROB). (2013). http://sidc.be/silso/datafiles

Rozanov, E., Egorova, T., & Schmutz, W. (2008). Response of the Earth's atmosphere to the solar irradiance variability. *Advances in Global Change Research*, *33*, 317–331.

Shevchuk, N. O., Ortikov, M. Y., & Pogoreltsev, A. I. (2018). Modeling of atmospheric tides with account of diurnal variations of ionospheric conductivity. *Russian Journal of Physical Chemistry B*, *12*(3), 576–589. https://doi.org/10.1134/S199079311803017X

Tapping, K. F. (1987). Recent solar radio astronomy at centimeter wavelength: The temporal variability of the 10.7-cm flux. *Journal of Geophysical Research*, *92*(D1), 829–838. https://doi.org/10.1029/JD092iD01p00829

Vadas, S. L., & Fritts, D. C. (2006). Influence of solar variability on gravity wave structure and dissipation in the thermosphere from tropospheric convection. *Journal of Geophysical Research*, *111*, A10S12. https://doi.org/10.1029/2005JA011510

Wang, J. C., Chang, L. C., Yue, J., Wang, W., & Siskind, D. E. (2017). The quasi 2 day wave response in TIME-GCM nudged with NOGAPS-ALPHA. *Journal of Geophysical Research: Space Physics*, *122*, 5709–5732. https://doi.org/10.1002/2016JA023745

Xiao, C., Xiong Hu, X., & Tian, J. (2009). Global temperature stationary planetary waves extending from 20 to 120 km observed by TIMED/SABER. *Journal of Geophysical Research*, *114*, D17101. https://doi.org/10.1029/2008JD011349

Yigit, E., & Medvedev, A. S. (2009). Heating and cooling of the thermo-sphere by internal gravity waves. *Geophysical Research Letters*, *36*, L14807. https://doi.org/10.1029/2009GL038507

Yigit, E., & Medvedev, A. S. (2010). Internal gravity waves in the thermosphere during low and high solar activity: Simulation study. *Journal of Geophysical Research*, *115*, A00G02. https://doi.org/10.1029/2009JA015106

Yoden, S. (1990). An illustrative model of seasonal and interannual variations of the stratospheric circulation. *Journal of the Atmospheric Sciences*, *47*, 1845–1853.

Zarubin, A. S., & Pogoreltsev, A. I. (2014). Analysis of gravity wave effects in the upper atmosphere using different parameterizations. *Izvestia VUZov, North-Caucasian Region, Natural Sci Series*, *2*, 35–39. (in Russian)